Available online at www.sciencedirect.com

ScienceDirect

Ciência & Tecnologia dos Materiais 27 (2015) 15–26

Ciência & Tecnologia dos MATERIAIS

http://ees.elsevier.com/ctmat

Special Issue PCF 2014

Embedment strength characterization of pine wood. Numerical study of the non-linear behaviour

Cristóvão L. dos Santos[a,b,*], Abílio M. P. de Jesus[c,d], José J. L. Morais[a,b]

[a] *Universidade de Trás-os-Montes e Alto Douro, UTAD, Escola de Ciências e Tecnologia, Quinta de Prados, 5001-801 Vila Real, Portugal*
[b] *CITAB, Universidade de Trás-os-Montes e Alto Douro, UTAD, Quinta de Prados, 5001-801 Vila Real, Portugal*
[c] *Faculdade de Engenharia da Universidade do Porto, Rua Dr. Roberto Frias, 4200-465 Porto, Portugal*
[d] *INEGI/LAETA, Rua Dr. Roberto Frias, 4200-465 Porto, Portugal*

Abstract

This paper presents experimental and numerical results from embedment tests carried out accordingly the EN383 standard. The experimental program included series of compressive embedment tests, along the parallel and perpendicular-to-grain directions. The specimens were manufactured with maritime pine wood and were loaded using a steel dowel. The load-displacement curves resulted from experimental tests allowed to estimate the embedding strength and the foundation modulus. Concerning the numerical simulations, a plasticity model, based on Hill's criterion, was used to simulate the mechanical behaviour observed in the embedment tests. The wood was modelled as an orthotropic material following an elasto-plastic behaviour. The steel dowel was considered isotropic material and modelled with elastic behaviour. Besides, the interaction between both materials was modelled using contact finite elements. A parametric study to evaluate the influence of dowel/wood clearance and different friction coefficients was performed. The proposed 3D finite element model showed the capability to simulate the non-linear behaviour observed in the experimental embedment tests. An experimental/numerical procedure for the identification of constitutive models aiming the simulation of ductile behaviour of wood was presented. This is particularly important to simulate the mechanical behaviour of doweled joints.

Keywords: maritime pine wood (*Pinus pinaster* Ait.); embedment tests; finite element analysis; Hill's plasticity model; hole/fastener clearance; friction.

1. Introduction

Currently in Europe, the EC5 design code [1] presents the procedures that allow the estimate of the strength of timber connections. The determination of the strength of connections requires prior knowledge of embedding strength of wood. This is particularly true for the ductile failure modes occurring in timber. The embedding strength can be determined using experimental tests conducted according to the EN383 standard [2]. This test method is based on the principle of reproducing the behaviour of doweled connections but with robust fasteners to minimize its bending. Also, the embedding strength can be calculated by means of empirical equations provided in EC5 design code. The embedment strength is the base information for joints design according to the European Yield Model (EYM), also referred to as Johansen model [3]. According to the EYM, embedding strength of wood is a material parameter governing the failure of wood members. This model has an empirical basis and assumes an elastic-perfectly plastic behaviour for both wood and dowel. It also considers that embedding strength is a material property, when in fact it is

* Corresponding author.
E-mail address: clsantos@utad.pt (C.L. dos Santos)

http://dx.doi.org/10.1016/j.ctmat.2015.04.003

non-unique for any given specimen of timber, depending on several factors, such as size, cross-sectional shape and surface condition of fastener, orientation of fastener with respect to timber grain, degree of initial contact between fastener and wood [4]. In order to study all possible variations of those factors, a number of experimental tests are required for assessing the embedding strength. A literature review shows the necessity of numerical approaches to investigate embedding strength more efficiently [5]. Thus, some 2D finite elements models have been proposed such as non-linear beam on foundation [6, 7] and finite element models (FEM) [6, 8-10]. However, it has been recognized that these models only give reasonable predictions for very specific extreme situations such as very thin or very thick wood members. Typically, doweled joints are three dimensional problems (non-uniform stress distributions across the member thickness). Therefore, it is necessary to use a 3D FEM to simulate the embedding behaviour of dowel-type connections.

Wood is an anisotropic material. When compressed along the parallel-to-grain direction it presents ductile compressive behaviour with softening. If wood is compressed along the perpendicular-to-grain direction it presents ductile behaviour but with hardening [11]. Therefore, an appropriate wood constitutive law is important for the simulation of non-linear behaviour resulting of embedding strength.

Currently, 3D-FEM with Hill´s plasticity model implementation has been successfully applied to simulate the non-linear behaviour of dowel-type wood connections. The plasticity of timber connections is well reproduced beyond the design limit conditions [12-15]. However, this approach is not able to simulate the collapse of timber connections characterised by brittle behaviour. Thus, different strategies were used to simulate non-linear behaviour of dowel-type wood connections, namely, using constitutive models and failure criteria for specific failure modes [16-19], and using Linear Elastic Fracture Mechanics [20-22]. Recently, a new approach involving mixed plasticity and cohesive damage modelling was presented to simulate both ductile and brittle behaviours that may coexist in dowel-type wood connections [23-25]. However, compressive embedment tests are characterized exclusively by ductile behaviours, due to wood crushing and densification beneath the dowel; therefore it is expected that the use of a plasticity model would be reasonable to model the embedment tests. Another interesting perspective is the possibility of using the embedment tests as a standard procedure to provide experimental data required to calibrate the parameters of the plasticity models that can afterwards be applied for timber connections simulation.

Given the previous framework, this paper presents experimental and numerical results from embedment tests performed according to the EN 383 standard [2]. The experimental program included two series of compressive tests, loaded both parallel and perpendicular-to-grain directions. The specimens were manufactured in maritime pine wood (*Pinus pinaster* Ait.), which is one of the species with large implantation in Portugal; the dowel was made of steel. The paper also presents a 3D-FEM numerical model that includes a plastic material representation, supported by Hill's criterion, available in ANSYS® [26]. This approach has also been followed by some authors [12-15]. This 3D-FEM uses same elastic properties and contact parameters, calibrated by Santos et *al.* [27].

Regarding the literature review, it should be noted that the majority of 3D – FEM models developed to simulate dowel-type wood connections, assume that hole and fasteners have same diameters. However, it is necessary to manufacture the hole in wood, slightly larger than the diameter of the dowel, in order to facilitate the installation and to allow for small misalignments of members [4,6]. The friction coefficient between the hole in wood and the metallic fastener also has influence in embedding strength determination [4,28]. In order to evaluate the influence of those parameters, this paper includes a parametric study considering both the dowel/hole clearance and friction as variables.

2. Experimental program

2.1. Experimental details

This paper presents results from embedding tests according to the EN383 standard [2]. Both parallel (longitudinal) and perpendicular-to-grain (radial) compressive embedment tests were carried out, as illustrated in Fig. 1. The nominal diameter of the dowel (d) was 14 mm, and the specimen thickness (t) was 30 mm. The dimensions of the specimens are proportional to the diameter of dowel (see Fig. 1), as proposed in the EN 383 standard. The distance between the inner faces of the side steel plates used in the embedment tests was 31.20 mm. Therefore, the average clearance between the specimen and the side steel plates at the beginning of the tests was

approximately 1.2 mm. Two series of tests were conducted as described in Table 1, namely longitudinal compression (LC) and radial compression (RC) tests.

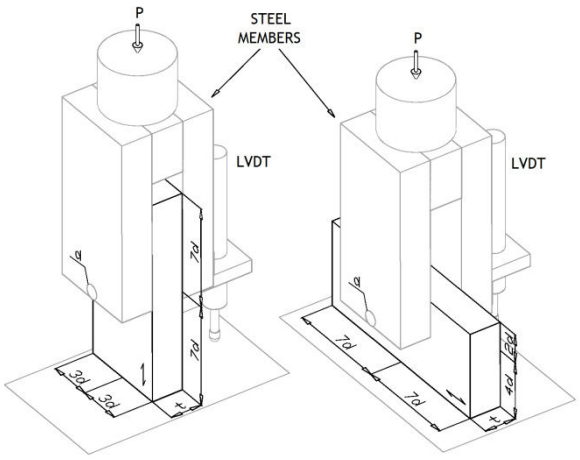

Fig. 1. Schematic representation of the embedment tests according to the EN383 standard [2]: (left) longitudinal compression; (right) radial compression.

The specimens used in the embedment tests were made of Maritime pine wood (*Pinus pinaster* Ait.), which is one of the most representative species of the Portuguese forest. The specimens were manufactured from trees harvested in the region of Viseu (Portugal). Trees with straight stems (absence of reaction wood) and diameters at breast height of approximately 400 mm were selected. Three meters long logs were cut from the sample trees between three and six meters above the basal plane. The logs were live-sawn into thick boards that were kiln-dried to a moisture content between 10% and 12%. The specimens were cut from these boards by aligning the parallel-to-grain direction with the length of the specimens and the wood tangential direction with the thickness of the specimens, as depicted in Fig. 2. Wood with knots, resin pockets, or other type of defects was excluded to reduce the usual scatter observed in embedment tests.

Tests were performed on an INSTRON® machine, model 1125, rated to 100 kN, under crosshead displacement control. Linear variable differential transducers (LVDT) were used to measure the relative displacement between the dowel and the base plate (see Fig. 1). The LVDTs used in the experimental program were from Applied Measurements® with reference AML/EU ± 10-S10 (measurement range of ±10 mm). The data were acquired by means of a SPIDER® 8-30 system. A loading-unloading-reloading procedure was adopted, as suggested in the EN 383 standard: first, specimens were loaded until 40% of the maximum estimated load (F_{est}), and the crosshead position was held for 30s; after this stage, specimens were unloaded until $0.1F_{est}$, and the crosshead position was again maintained for 30s; finally, specimens were reloaded until failure. The maximum load was initially estimated based on preliminary tests; afterwards, this load was updated after each test (Table 1).

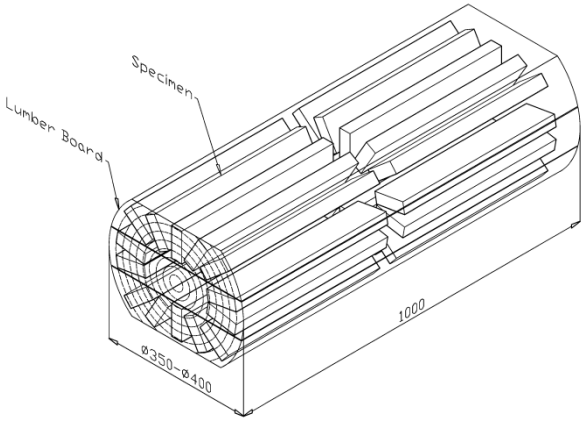

Fig. 2. Procedure for the selection of specimens from a tree trunk.

Table 1. Summary of embedding tests

Series	Number of specimens	Displacement rate (mm.min^{-1})	$F_{max,est}$ (N)	Density (kg.m^{-3})
LC	24	0.3	18000	570.1±38.3
RC	24	1.0	8000	550.1±49.0

2.2. Embedding test results and discussion

Fig. 3 illustrates the load-displacement curves obtained for the two embedding test series, where displacements are relative to the dowel and were measured using LVDTs. An analysis of the Fig. 3a reveals that the longitudinal embedding tests are characterised by load-dowel displacement curves with a load plateau, where the maximum load may be clearly identified. The load plateau was followed by an abrupt load drop due the cracks initiation and propagation below the dowel leading to the collapse of the specimen (see Fig. 5). For the sake of clarity, Fig. 3a only represents the results until the load drop, the abrupt loading drop being omitted. The maximum load and the load plateau were consequently well defined in the Fig. 3a. It is observed a significant scatter in the

ultimate displacements that preceded the crack initiation and propagation. The failure modes will be illustrated latter in the paper supported by Fig. 5. The radial compression tests exhibit a monotonically increasing loading beyond the proportional limit (see Fig. 3b). Based on the analysis of Fig. 3 it is possible to establish typical load-displacement curves for the embedding tests, as depicted on Fig. 4. Fig. 4a corresponds to the longitudinal compression tests and defines an ultimate load (F_u) as well as an initial stiffness (k_1). Fig. 4b, corresponding to the radial compression tests, illustrates a load-displacement record by two line segments with distinct slopes (k_1 e k_2). Since it is not possible to define an ultimate load, a load beyond the proportional limit range ($F_{0.05d}$) is adopted, corresponding to a residual displacement of 5% the diameter of the dowel [29].

The previous referred parameters can be normalized, dividing their values by the projected area of the hole, resulting the embedding strength (f_h) and foundation modulus (K_i):

$$f_h = \frac{F}{d.t} \quad (1)$$

$$K_i = \frac{k_i}{d.t} \quad (2)$$

where: d is the diameter of the dowel, t the thickness of the specimen, F the ultimate (F_u) or the load beyond the proportional limit range ($F_{0.05d}$) and k_i the initial (k_1) or final stiffness (k_2). Table 2 summarizes the global values of embedding strength and foundation modulus measured for each test series. The f_h and K_1 values are significantly higher in the longitudinal compression tests than in the radial compression tests. While f_h is about two times higher in longitudinal compression than in radial compression, K_1 is approximately three times higher in longitudinal compression than in radial compression. Significant correlations were measured (not shown here, consult [27] for details) between the embedding strength and wood densities; the correlation was poor for the foundation modulus, perhaps due to low range of experimental densities.

Fig. 5 illustrates the damage evolution observed in embedding test series, leading to distinct failure modes, which depends on wood directions. In general, bearing and shear splitting failures are observed. The plane in which the shear splitting occurs is the plane defined by the longitudinal and tangential directions (LT plane). For longitudinal compression tests, the failure starts with fibres crushing beneath the dowel, being the load in a plateau around the maximum load. After some amounts of deformation, the final failure occurs due to the formation of one or two shear splitting cracks, leading to an abrupt loss of loading. The radial compression tests are characterised by a densification of the wood beneath the dowel, due to the collapse of the wood cells, mainly from the early wood.

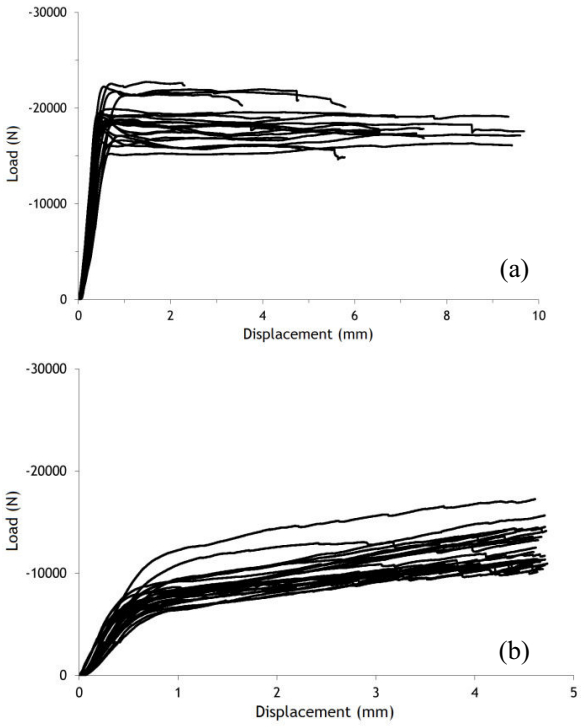

Fig. 3. Load-displacement curves: (a) longitudinal compression; (b) radial compression.

Table 2. Summary of experimental results from the embedding tests [27]

Series	f_h (MPa)	K_1 (N.mm^{-3})	K_2 (N.mm^{-3})
LC	46.4±4.2	113.3±23.5	
RC	21.1±3.6	37.2±8.8	3.1±0.74

3. Numerical simulation

3.1. Overview of previous linear elastic analysis

This paper presents results from numerical simulation of embedment tests. In this section an overview of previous elastic analysis performed by authors [27] is presented. The models developed for the elastic analysis were later updated with a non-linear constitutive model for wood and results presented in Section 3.2.

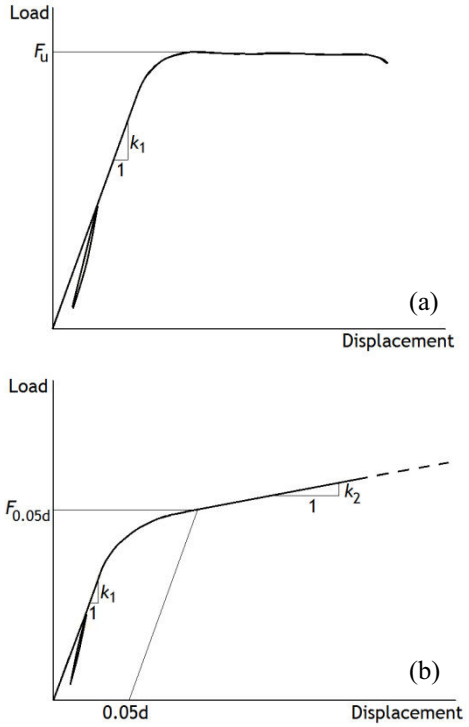

Fig. 4. Typical load-displacement curves and associated parameters: (a) longitudinal compression; (b) radial compression.

Three dimensional FE models were built using the commercial code ANSYS® 12.0 through the ANSYS Parametric Design Language (APDL language) [26]. Models composed by two solids, namely the wood specimen and the steel dowel, were created using 20-noded hexahedra isoparametric elements (SOLID95). Given that test configurations present two planes of symmetry, only ¼ of the global geometry was modelled. The displacements of the nodes placed at the symmetry planes were restrained in a direction normal to these planes. The contact between the dowel and the wood specimen was modelled with contact elements available in ANSYS elements library. A surface-to-surface contact technology was chosen, together with a contact pair defined by the CONTA174 and the TARGE170 elements. Both surfaces coming into contact were considered flexible, namely the hole surface in the wood specimen and the dowel surface. The Augmented Lagrange contact algorithm and the basic Coulomb friction model were used. For the proposed simulations, were adopted the contact parameters calibrated by authors on previous elastic simulations of embedding tests along the longitudinal and radial directions, performed on similar wood members [27]. The maximum penetration factor, FTOLN = 0.1 was used for dowel-wood contact in both compressive tests and the normal contact stiffness was assumed FKN=0.1 or FKN=0.006, respectively, for parallel or perpendicular-to-grain loading.

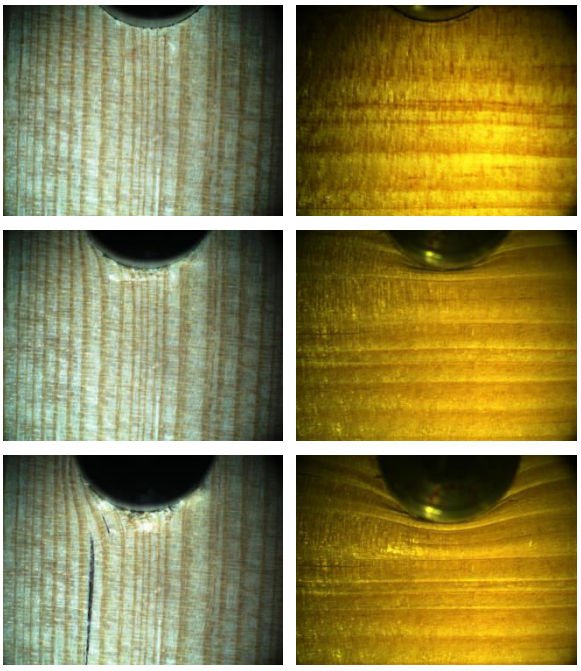

Fig. 5. Damage evolution for specimens during the loading: (left) longitudinal compression; (right) radial compression.

In linear elastic analysis, both materials were modelled as elastic and homogeneous. The steel of the dowel was assumed isotropic (E = 210 GPa, ν= 0.3). Wood was assumed orthotropic, with the nine independent elastic constants summarised in Table 3. Regarding the simulations performed by Santos et *al.* [27], two distinct support conditions for the dowel were assumed: simply supported dowel and perfectly clamped dowel. Better numerical results were obtained when the simply supported dowel conditions were adopted, so, in present study only these conditions were modelled. The simply supported conditions were simulated using an extra contact pair established between the outer surface of the ends of the dowel (flexible surface) and a rigid plate (rigid-flexible contact pair). The clearance between dowel and holes was assumed equal to 0.3 mm which is an average value from experimental measurements. The friction coefficient was assumed equal to 0.5, which has been considered a typical value for steel/wood contact. In spite of linear elastic materials, the global problem is non-linear due to the contact elements, requiring an incremental load stepping. For all simulations, a displacement of 0.1 mm was applied to the dowel ends or to the rigid loading plane,

according to 10 equal increments. Taking into account the two loading directions, two 3D-FEM models were developed. Fig. 6 illustrates the details of FE meshes used in the simulations.

This first analysis revealed an unsatisfactory description of experimental results since the observed experimental non-linear behaviour of the joint is not captured by the simulation [27]. A literature review about numerical modelling of wood non-linear behaviour [12-18] reveals plasticity constitutive models as a satisfactory option.

Table 3. Elastic properties of Maritime pine [27]

E_L = 15.1 GPa	ν_{LR} = 0.47	G_{LR} = 1283 MPa
E_R = 1.91 GPa	ν_{RT} = 0.59	G_{RT} = 264 MPa
E_T = 1.01 GPa	ν_{TL} = 0.05	G_{TL} = 1117 MPa

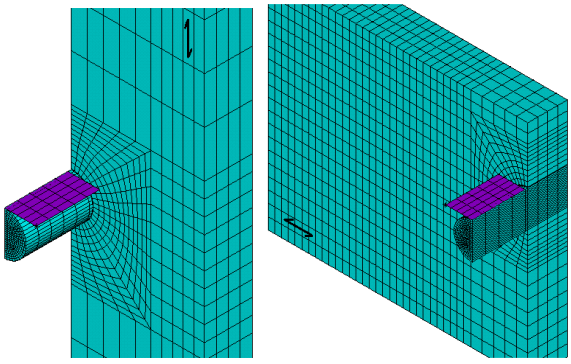

Fig. 6. 3D-FE meshes of the tests: (left) longitudinal compression; (right) radial compression.

3.2. Non-linear elasto-plastic analysis

After the initial linear elastic analysis demonstrated the inability of simulating the global non-linear behaviour observed in the embedment tests, a non-linear constitutive model was proposed for wood. However previous work was very helpful to propose the base model for the following non-linear analysis. Besides the material non-linearity, non-linear geometric behaviour was also considered due to the large deformations. The ANSYS® code [26] offers a constitutive plasticity model for anisotropic materials, based on Hill's yield criterion that was used in this work to model wood [30]. The Hill criterion is an extension of the von Mises yield criterion, to account for the anisotropic yield of the material. When this criterion is used with the isotropic hardening option, the yield function is given by:

$$f = \sigma_{eq} - \sigma_0 = \sqrt{\{S\}^T[M]\{S\}} - \sigma_0 = 0 \qquad (3)$$

were: σ_{eq} is the equivalent stress, $\{S\}$ is the deviatoric stress, σ_0 is the reference yield stress and $[M]$ is the plastic compliance matrix that takes into account the material anisotropy. The material is assumed to have three orthogonal planes of symmetry. Assuming the material coordinate system perpendicular to these planes of symmetry (orthotropic material), the plastic compliance matrix $[M]$ can be written as:

$$[M] = \begin{bmatrix} M_2+M_3 & -M_3 & -M_2 & 0 & 0 & 0 \\ -M_3 & M_1+M_3 & -M_1 & 0 & 0 & 0 \\ -M_2 & -M_1 & M_1+M_2 & 0 & 0 & 0 \\ 0 & 0 & 0 & 2M_6 & 0 & 0 \\ 0 & 0 & 0 & 0 & 2M_4 & 0 \\ 0 & 0 & 0 & 0 & 0 & 2M_5 \end{bmatrix} \qquad (4)$$

where M_1, M_2, M_3, M_4, M_5 and M_6 are material constants that can be determined experimentally. They are defined as:

$$M_1 = \frac{1}{2}\left(\frac{1}{R_{yy}^2} + \frac{1}{R_{zz}^2} - \frac{1}{R_{xx}^2}\right) \qquad (5)$$

$$M_2 = \frac{1}{2}\left(\frac{1}{R_{zz}^2} + \frac{1}{R_{xx}^2} - \frac{1}{R_{yy}^2}\right) \qquad (6)$$

$$M_3 = \frac{1}{2}\left(\frac{1}{R_{xx}^2} + \frac{1}{R_{yy}^2} - \frac{1}{R_{zz}^2}\right) \qquad (7)$$

$$M_4 = \frac{3}{2}\left(\frac{1}{R_{yz}^2}\right) \qquad (8)$$

$$M_5 = \frac{3}{2}\left(\frac{1}{R_{xz}^2}\right) \qquad (9)$$

$$M_6 = \frac{3}{2}\left(\frac{1}{R_{xy}^2}\right) \qquad (10)$$

were R_{xx}, R_{yy}, R_{zz}, R_{xy}, R_{yz} e R_{xz} are anisotropy coefficients, which are defined as the ratio between the yield stress in each direction, σ_{ij}^y, and the reference yield stress, σ_0, corresponding to a specific direction:

$$R_{xx} = \frac{\sigma_{xx}^y}{\sigma_0} \qquad (11)$$

$$R_{xy} = \sqrt{3}\frac{\sigma_{xy}^y}{\sigma_0} \qquad (12)$$

$$R_{yy} = \frac{\sigma_{yy}^{y}}{\sigma_0} \quad (13)$$

$$R_{yz} = \sqrt{3}\frac{\sigma_{yz}^{y}}{\sigma_0} \quad (14)$$

$$R_{zz} = \frac{\sigma_{zz}^{y}}{\sigma_0} \quad (15)$$

$$R_{xz} = \sqrt{3}\frac{\sigma_{xz}^{y}}{\sigma_0} \quad (16)$$

The Hill's plasticity model is based in a yield convex surface represented in the stress space (Haigh-Westergaard space). When the material is in elastic domain, the condition $f < 0$ is verified; in a process with plastic deformation, it follows that $f = 0$ and $df = 0$. The flow rule determines the plastic strain increment $\{d\varepsilon^P\}$ by means of the following equation:

$$\{d\varepsilon^P\} = \lambda\left\{\frac{\partial Q}{\partial \sigma}\right\} \quad (17)$$

were λ is the plastic multiplier and Q is a function of the stress, termed the plastic potential. In this study associate plasticity was adopted, so the plastic potential is considered the same as the yield function ($Q = f$).

During a plastic deformation process, occurs an evolution of the yield surface, in order to ensure permanently the condition $f = 0$. In this study, an isotropic hardening model was adopted since monotonic behaviour of wood is investigated. The yield surface is allowed to expand around a fixed centre, when the plastic strain occurs. The yield surface is function of the plastic work, k, that controls the diameter of the yield surface, σ_0:

$$f = \sqrt{\{S\}^T[M]\{S\}} - \sigma_0(k) = 0 \quad (18)$$

The plastic work is considered a state variable of the constitutive model, and can be determined by means of the following equation, that represents the plastic work along the loading history:

$$k = \int\{\sigma\}^T[M]\{d\varepsilon^p\} \quad (19)$$

In this study was adopted a linear rule for $\sigma_0(k)$, which causes uniaxial stress-strain relations, with the configuration illustrated in Fig. 7. The proposed model considers symmetric tension/compression behaviours. This hardening rule allows the simulation of a perfectly plastic behaviour, which is a particular case of the behaviour illustrated in Figure 7.

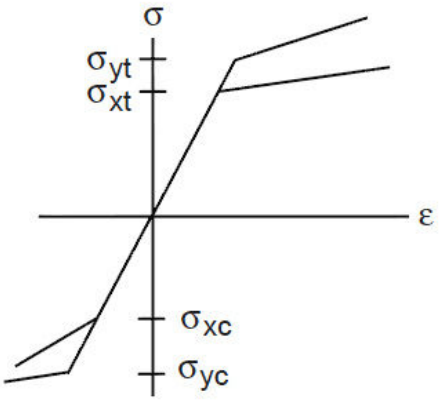

Fig. 7. Uniaxial stress-strain curves simulated by the anisotropic Hill's plasticity model with isotropic hardening [26].

In order to implement the plasticity model, a reference non-linear uniaxial stress-strain curve must be established. Also, anisotropic stress ratios (see Eqs. 11-16) are required in order to allow the transformation of the reference curve into material curves for simple loading directions (tension/compression and shear). The standard Hill's model used in this paper does not distinguish tension from compression behaviours of wood. Therefore, the model calibration requires a compromise between these two distinct wood behaviours, taking into account the dominant stress states applied on wood specimens. Since the plasticity model, based on Hill's yield criterion, is adopted to simulate the embedment tests, the resulting model constants will be suitable to model wood under dominant compression stresses. This condition is characteristic of doweled wood connections where the non-linear behaviour of these structural details arises from the non-linear compressive behaviour of wood.

The material was simulated as transversely isotropic and the reference curve was assumed perfectly plastic. Therefore, the anisotropic stress ratios required for the model identification corresponded in practice to ratios between anisotropic yield stresses. Two alternative approaches were followed for the elasto-plastic analysis:

i) Distinct plasticity model parameters were identified for each one of the two series of embedment tests (see Table 4). This approach propose independent plasticity parameters adjusted for each wood direction (parallel and perpendicular-to-grain) in a tentative to produce better global predictions of the mechanical behaviour of the embedment tests. This approach could be interesting if one want to simulate a doweled

wood joint for which the load direction in each member is known in advance. For these cases one may select the better set of constants to simulate the member's behaviour.

ii) The same plasticity model parameters were used for both embedment tests series (see Table 5). This approach is physically more consistent since the materials of each tested series are the same. This approach is interesting for the simulation of dowelled joints where load direction in each member is unknown or involves a loading direction not covered by the performed embedment tests.

Tables 4 and 5 presents the yield stresses for tension/compression and shear simple (uniform) stress states. Using these yield stresses, the anisotropic ratios were defined taking into account an arbitrary reference curve. Besides the yield stresses adopted for the plasticity model, strength properties extracted from experimental works performed on the same wood species and available in the literature [30], are also presented in the referred tables. These strength properties were used to estimate the yield stresses. The experimental strength properties were presented for both longitudinal tension and compression loading. For radial and tangential directions, only compression strengths were given in the tables (one value for each direction). Concerning the shear strengths, a range of experimental values are given, which resulted from alternative shear testing experiments [31, 32]. The yield stress values used in these simulations, for the various material directions are summarized in Tables 4 and 5. Table 4 refers two distinct sets of constants identified respectively with each embedment test data (longitudinal compression (LC) and radial compression (RC)). Table 5 presents the model constants that were identified using simultaneously the radial and longitudinal compression tests. All plasticity parameters were defined taking into account the experimental values as reference.

Concerning the clearance between the dowel and hole, the value of 0.3 mm was maintained. However, when the plasticity model was implemented, friction coefficient started to influence the numeric results significantly, particularly in the longitudinal embedment tests. Thus, friction coefficient was decreased to 0.3 in order to produce more consistent simulation results. Furthermore, a parametric study about the influence of clearance and friction coefficient is presented, showing the influence of these parameters on the numerical simulation of the embedment tests.

Table 4. Experimental strength properties and adopted yield values for Pine wood: distinct constants used for each wood member

		Tension/ Compression		Shear		
		L	R / T	LR	RT	LT
Experimental strength values (MPa)		40–98	4.2–9.4	14–16	2.4–4.5	14–16
Adopted yield stresses (MPa)	LC	90	5.3	12.8	4.1	14.4
	RC	85	5.3	11.2	3.2	11.2

Table 5. Experimental strength properties and adopted yield values for Pine wood: same constants set used for both wood members

		Tension/ Compression		Shear		
		L	R / T	LR	RT	LT
Experimental strength values (MPa)		40–98	4.2–9.4	14–16	2.4–4.5	14–16
Adopted yield stresses (MPa)	LC	80	6.1	12.8	3.6	12.8
	RC					

The numerical load-displacement curves with the better approximation to experimental curves are presented in Fig. 8. This satisfactory approximation resulted from the application of distinct sets of plastic constants for each one of the embedment tests (constants from Table 4). In a second approach, the same set of plasticity parameters were used for both tests simulation (constants set of Table 5). This later approach is physically more consistent since the material used in both embedment tests was the same. However, after filtering some scatter in experimental results, particularly in longitudinal direction, a good compromise between experimental and numerical load-displacement curves is reached, as depicted in Fig. 9. The initial stiffness, in the linear region, is well reproduced, confirming good performance of the contact model that was calibrated in the linear elastic analysis, as well as a good estimate of the elastic properties.

The yield transitions are well reproduced, being progressive in the radial compressive tests and more abrupt, with an initial peak, in longitudinal compressive tests. After yield transition, the hardening non-linear behaviour was satisfactorily reproduced for both longitudinal and radial compression tests.

The numerical load-displacement curves were horizontally shifted so the initial contact embedding

observed in the experimental results was avoided. This corresponded to horizontal shifts of 0.1 mm and 0.05 mm, in CL and CR tests, respectively. The maximum value simulated for the applied displacement was 4 mm. This value is well beyond the design conditions, corresponding to a displacement value for which the damage in wood is very significant. The finite elements presented a significant distortion, when subjected to these values of displacement.

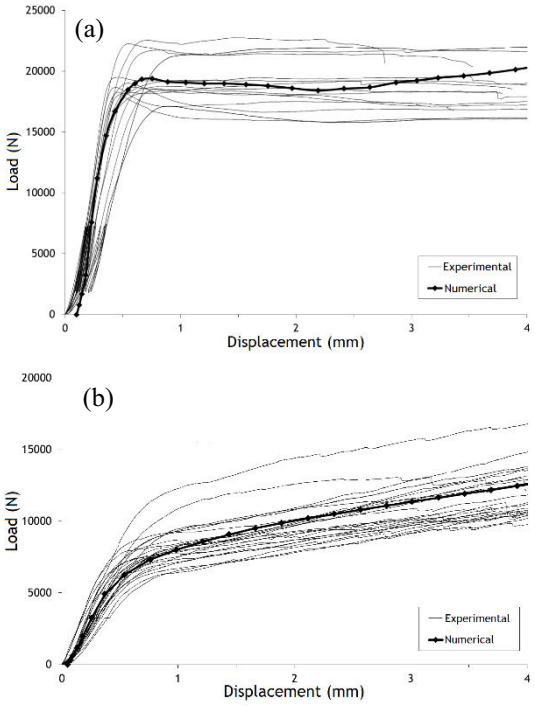

Fig. 8. Experimental vs. numerical F-d curves obtained with distinct sets of plasticity parameters: (a) longitudinal compression; (b) radial compression.

Figs. 10 and 11 illustrate, respectively, the displacement and stress fields, for both embedment tests simulation, for three distinct stages of the applied displacements. The selected loading stages are identified in Fig. 9, by the points (a), (b) and (c), for longitudinal compressive tests, and (d), (e) and (f), for radial compressive tests. These points try to illustrate the behaviour of wood for the elastic limit, intermediate yield condition and post-yield condition.

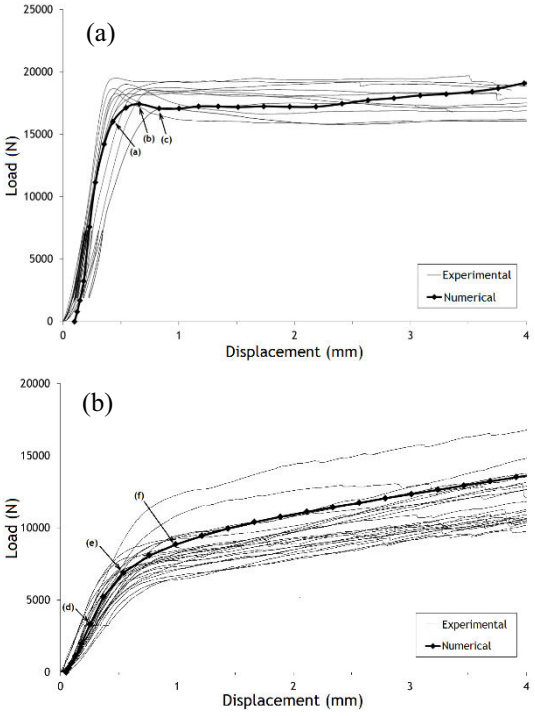

Fig. 9. Experimental vs. numerical F-d curves obtained with same set of plasticity parameters: (a) longitudinal compression; (b) radial compression.

The plasticity model with constants from Table 5 was used in the 3D-FEM model. The displacement field evaluated beneath the hole (see Fig. 10) showed an uniform distribution for longitudinal compressive tests, in all three loading stages; in radial compressive tests, at the elastic limit, the displacements field is more intense near the side faces of the specimen. However, it tends to uniformity along the specimen thickness with increasing loading and consequently with increasing embedding.

Concerning the stress distributions (see Fig. 11), the direct stresses, σ_R, for radial compressive tests and the shear stresses, τ_{RL}, for longitudinal compressive tests were represented. The analysis of Fig. 11 shows that stress distributions are more uniform for simulations of embedment tests performed according the parallel-to-grain direction. The embedment tests according perpendicular-to-grain directions reveal significant tensile stress at the middle horizontal plan of the hole. Also it is verified non-uniformity across thickness of the stress distributions which is a clear indication of the need of a 3D model to simulate accurately the embedment tests.

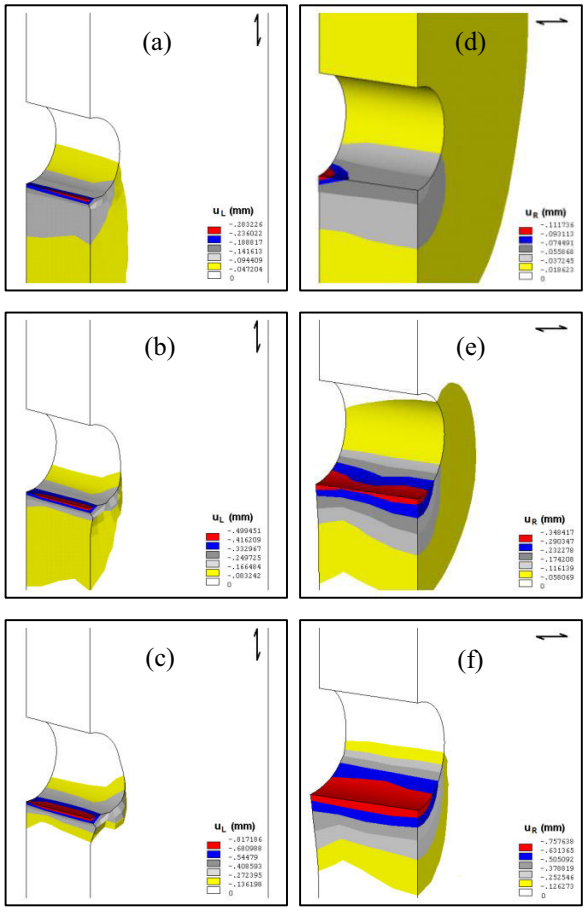

Fig. 10. Displacement fields from 3D-FEM model: (a) (b) (c) U_L displacements for LC series; (d) (e) (f) U_R displacements for RC series.

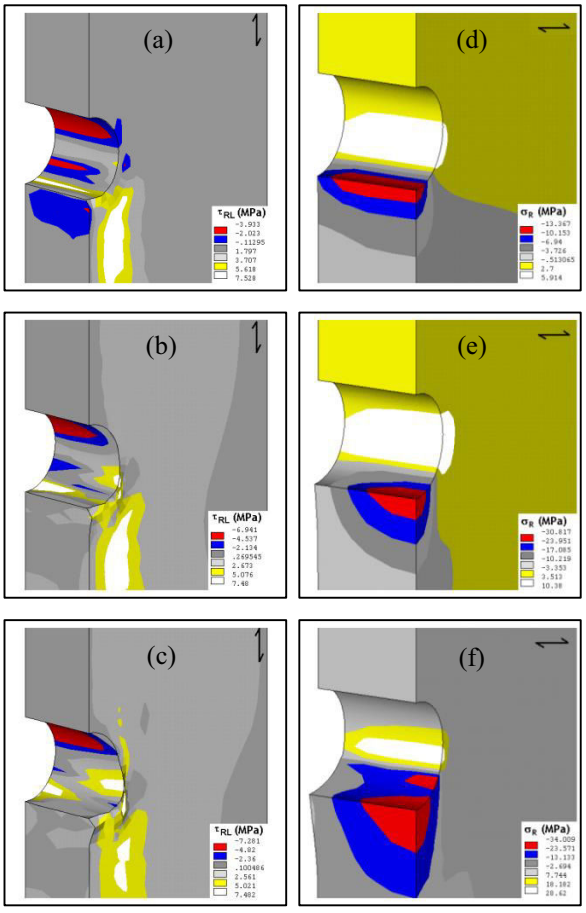

Fig. 11. Stress fields from 3D-FEM simulations: (a) (b) (c) τ_{RL} stresses for LC series; (d) (e) (f) σ_R for RC series.

3.3. Friction coefficient and dowel/hole clearance effects

The 3D-FEM model developed to simulate the embedment tests, demonstrates important sensitivity when occurs variation of friction coefficient between steel and wood (μ), as well as with the variation of the clearance between the hole and the dowel. Thus, it is important to control these two parameters in design of wooden connections. Generally, the holes obtained in the wood members present low dimensional and geometric precision, with variable roughness on surface due to wood anatomy. Along time, humidity absorption or loss, in the timber, also causes changes in volume, originating directly, dimensional and geometrical variations in the holes of joints.

Regarding the steel dowels, these can be manufactured with good dimensional and geometric precision; also its roughness can be controlled.

Experimentally is difficult to understand the interaction of these parameters, clearance and μ. Thus, using the developed 3D-FEM model, a parametric study involving both parameters was performed.

Fig. 12 depicts numerical load-displacement curves, resulted from the application of different clearance values and distinct friction coefficients. The load-displacement curves obtained from the previous non-linear elasto-plastic analysis were maintained (clearance=0.3 mm; μ=0.3), in order to expose the influence of both parameters.

From the analysis of Fig. 12, it was evident that numerical modelling resulted in direct load capacity increase of the compressive tests, when null values of clearance are adopted. This effect is more evident in longitudinal compressive tests. According to the results, a reduction in clearance value also conducts to slight increase of stiffness, for compression in the radial direction. Therefore, it is clear that there must be control over the clearance between fastener and

hole since it has a no negligible effect on embedding strength. In general the clearance control is deficient since the adjustment between steel dowels and holes in wood, using standard dowels (with fixed diameter) is dependent on the low dimensional stability of the hole, caused either by the volume variation of timber or by its anatomy. The solution to this problem involves the application of reinforcements in the areas of holes, so that it is possible to drill with more precision, or alternatively, by the use of elastic dowels, i.e. that adjust to holes of variable diameter. However, the choice of elastic dowels can be discouraged since it can introduce high levels of stress, which in turn can conduct to initiation of cracks occurring in the wood.

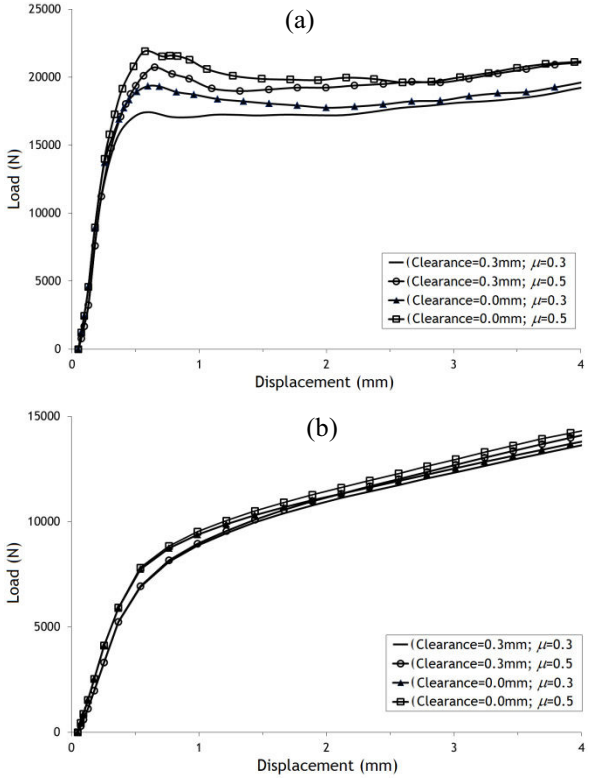

Fig. 12. Numerical F-D curves obtained for different clearance values and distinct friction coefficients: (a) longitudinal compression; (b) radial compression.

The variation of the friction coefficient also influenced the numerical results, which is particularly true in yield transition region and after yield process, see Fig. 12. This effect is more visible in simulation of embedment tests along the parallel-to-grain direction, as depicted in Fig. 12a. Friction coefficient is a parameter difficult to control experimentally, however, can be improved by using more rough or grooved dowels.

4. Conclusions

This paper presented results of embedding tests carried out according to the EN383 standard. Both embedding strength and foundation modulus were evaluated for *Pinus pinaster* wood species. Results demonstrated that the embedding strength, in radial direction, is significantly lower than corresponding value in longitudinal direction. The failure modes observed for the embedding tests corresponded to the local crushing and to the shear splitting according the LT planes.

3D finite element models, with contact pairs between the hole and the dowel, were built for simulating embedding tests proposed in EN383 standard procedures. A linear elastic analysis allowed the identification of relevant parameters of the modelling, namely the contact parameters. Additionally, a Hill's plasticity model was implemented. Contrarily to the observed with the elastic simulations, the friction coefficient had non-negligible influence on simulation results, in particular a significant influence in yield transition of the load-displacement curves of embedment tests was observed. The hole/dowel clearance continued to be determinant in the numerical results. These findings show the importance that of local reinforcements may represent in particular to provide dimensional and surface roughness, between the pair hole-dowel.

With distinct sets of plasticity parameters identified independently for both wood direction (parallel and perpendicular-to-grain), very good approximations were obtained to the same experimental load-displacement curves. The use of a unique set of plastic constants, despite physical consistent, led to a poorer load-displacement curves representation; however results are still quite satisfactory.

The embedment tests can be used as a standard procedure to provide experimental data for plasticity models calibration. These models are important for those interested to simulate doweled-wood connections, where the compressive behaviour of wood is the dominating damage process. However the plasticity models may be applied together with cohesive zone damage models to simulate cracking of wood joints, but the latter would require fracture mechanics tests for their identification.

References

[1] CEN1995-1-1. Eurocode 5: Design of timber structures - Part 1-1: General rules and rules for buildings, CEN/TC 250/SC5 (2004).
[2] CEN383. Timber Structures - Test methods - Determination of embedment strength and foundation values for dowel type fasteners. European Committee for Standardization (2007).
[3] K.W. Johansen, International Association for Bridge and Structural Engineering. *IABSE Journal* **9**, 249 (1949).
[4] T. Zhou, Z.W. Guan, *Prog. Struct. Engng Mater*. **8**, 49 (2006).
[5] T. Zhou, Z.W. Guan, *Constr. Build. Mater.* **25(2)**, 598 (2011).
[6] M. Patton-Mallory, P.J. Pellicane, F.W. Smith, *J. Struct. Eng*. **123**, 1054 (1997).
[7] K. Sawata, M. Yasamura, *J. Wood Sci.* **49**, 83 (2003).
[8] C.J. Chen, T.L. Lee, T.L., D.S. Jeng, *Comput. Struct.* **81**, 2731 (2003).
[9] P. Racher, J.F. Bocquet, *Electron J. Struct. Eng.* **5**, 1 (2005).
[10] N. Kharouf, G. McClure, I. Smith, *Comput. Struct.* **81**, 747 (2003).
[11] A. Reiterer, S.E. Stanzl-Tschegg, *Mech. Mater.* **33,** 12, 705 (2001).
[12] B.H. Xu, A. Bouchaïr, M. Taazount, P. Racher, *Constr. Build. Mater.* **23**, 3043 (2009).
[13] A.M.P.G Dias, J.W.G. Van de Kuilen, H.M.P. Cruz, S.M.R. Lopes, *Wood Fiber Sci.* **42**, 480 (2010).
[14] J-P. Hong, J.D. Barrett, F. Lam, *J. Wood Sci.* **57**, 119 (2011).
[15] M. Oudjene, M. Khelifa, *Constr. Build. Mater.* **23**, 11, 3359 (2009).
[16] D.M. Moses, H.G.L. Prion, *Can. J. Civil. Eng.* **30**, 555 (2003).
[17] D.M. Moses, H.G.L. Prion, *Compos. Part B-Eng.* **35**, 251 (2004).
[18] M. Patton-Mallory, S.M. Cramer, F.W. Smith, P.J. Pellicane, *J. Struct. Eng.* **123**, 1063 (1997)
[19] B.H. Xu, A. Bouchaïr, M. Taazount, P. Racher, *J. Wood Sci.* **59**, 17 (2013)
[20] M. Yasumura, L. Daudeville, *J. Wood Sci.* **46**, 187 (2000).
[21] M. Ballerini, M. Rizzi, *Mater. Struct.* **40**, 1, 139 (2007).
[22] L. Daudeville, M. Yasumura, *Mater. Struct.* **29**, 418 (1996).
[23] E. Resch, M. Kaliske, *Computers and Structures* **88**, 165 (2010).
[24] E. Resch, M. Kaliske, *Engineering Structures* **41**, 234 (2012).
[25] C.L. Santos, J.J.L. Morais, A.M.P. de Jesus, *Frattura ed Integrità Strutturale* **31**, 23 (2015).
[26] R. Hill, A theory of the yielding and plastic flow ofanisotropic metals, Proceedings of the Royal Society of London, Series A, Vol. 193, No. 1033, 1948, pp. 281-297.
[27] C.L. Santos, A.M.P. de Jesus, J.J.L. Morais, J.L.P.C. Lousada, *Strain.* **46**, 159 (2010).
[28] J. Sjodin, E. Serrano, B. Enquist, *Holz Roh Werkst.* **66**, 363 (2008).
[29] W. Munoz, A. Salenikovich, M. Mohammad, P. Quenneville, Determination of yield point and ductility of timber assemblies: in search for a harmonized approach, Proc. of Meeting 41 of CIB-W18, Canada, St Andrews, 2008.
[30] A.M.P de Jesus, A.M.V. Lima, J.J.L. Morais, J.L.C. Lousada, An investigation on compressive quasi-static behaviour of pine wood, 10th Portuguese Conference on Fracture, Guimarães, 22-24th February, 2006.
[31] J.C. Xavier, N.M. Garrido, M. Oliveira, J.L. Morais, P.P. Camanho, F. Pierron, *Composites: Part A.* **35**, 827 (2004).
[32] J.C. Xavier, M. Oliveira, J.L. Morais, T. Pinto, *Holzforschung* **63**, 217 (2009).